Astron. Astrophys. 332, 1035–1043 (1998)

ASTRONOMY
AND
ASTROPHYSICS

The molecular cloud core M 17-North: ISO spectroscopy and IR/mm continuum mapping⋆

Th. Henning[1], **R. Klein**[1], **R. Launhardt**[1], **D. Lemke**[2], **and W. Pfau**[1]

[1] Astrophysical Institute and University Observatory (AIU) Jena, Schillergäßchen 2-3, D-07745 Jena, Germany
[2] Max-Planck-Institute for Astronomy, Königstuhl 17, D-69117 Heidelberg, Germany

Received 21 July 1997 / Accepted 5 January 1998

Abstract. We present the first complete infrared spectrum of a molecular cloud core covering the wavelength region from 2.4 up to 200 μm together with a map at 1.3 mm wavelength and near-infrared (NIR) images. The core is located in the northern part of M 17 and shows strong evidence for on-going star formation. These data are the first step towards a complete characterization of M 17-North.

The spectrum has been obtained with the Infrared Space Observatory (ISO) using the short- and long-wavelength spectrometers (SWS/LWS) with a resolution from 150 to 300. The spectrum of the core displays the unidentified infrared bands (UIBs). The continuum is rising rapidly for wavelengths larger than 15 μm which is typical for objects with stronger UV radiation fields. This continuum is probably produced by the emission from very small grains (VSGs) heated transiently.

Many low-excitation fine structure lines were detected which are typical for the emission from an H II region. They are produced by an electron gas with a density and temperature of about 100 cm^{-3} and 5000 K, respectively.

The mapping of the continuum radiation at 1.3 mm revealed the presence of a compact cloud core, whereas NIR imaging led to the detection of embedded IR objects. The observed spectral energy distribution (SED) is used to model the cloud core emission with radiative transfer (RT) calculations including the emission from VSGs. This calculation shows that the cloud core is mainly heated by an outer radiation field but needs an additional inner heating source with a luminosity of about 8000 $\mathrm{L}_\odot$ to explain the measurements.

Key words: ISM: clouds – dust, extinction – ISM: individual objects: M 17N – infrared: ISM: continuum – infrared: ISM: lines and bands – radio continuum: ISM

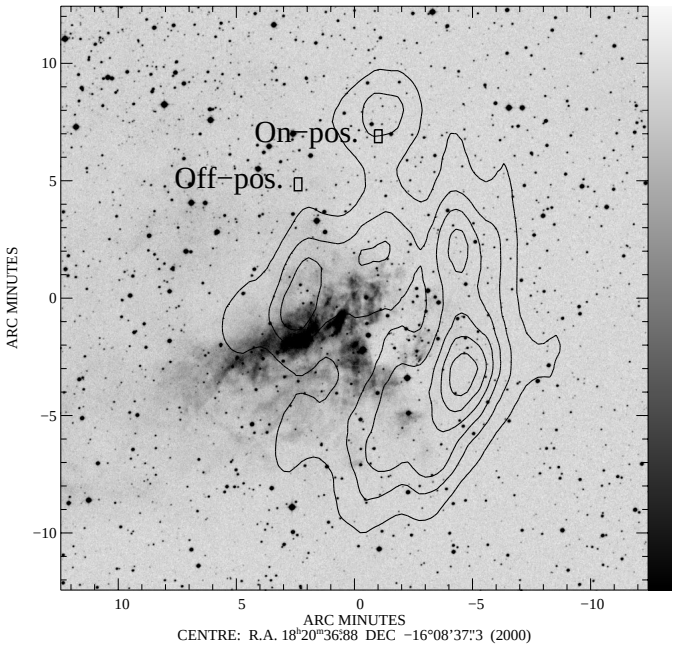

Fig. 1. M 17 in the V-band (DSS) with the contours of the IRAS-HiRes map at 100 μm. The contours are equally spaced between the maximum (45400 MJy/sr) and the minimum (240 MJy/sr) brightness. The maximum brightness in M 17-North is 17000 MJy/sr. The observed positions are displayed by boxes with the size and orientation of the largest SWS slit projected on the sky.

1. Introduction

M 17 is one of the best-studied regions of massive star formation in our galaxy (Stutzki et al. 1988). It is located in the Carina spiral arm at a distance of 2.2 kpc (Chini et al. 1980). The region is associated with an optically bright H II region which is partially surrounded by the bowl-shaped molecular cloud M 17-SW. Many studies of the central part of M 17 were performed, where the H II region, the bright molecular cloud cores, and the interface regions are located.

In contrast, the cloud core M 17-North located 10′ north of the exciting stars of M 17 was investigated only by low-resolution studies of the whole cloud complex (e.g., Gatley et al. 1979; Wilson et al. 1979). Fig. 1 shows the contours of the

Send offprint requests to: rklein@astro.uni-jena.de

⋆ Based on observations with ISO, an ESA project with instruments funded by ESA Member States (especially the PI countries: France, Germany, the Netherlands and the United Kingdom) with the participation of ISAS and NASA

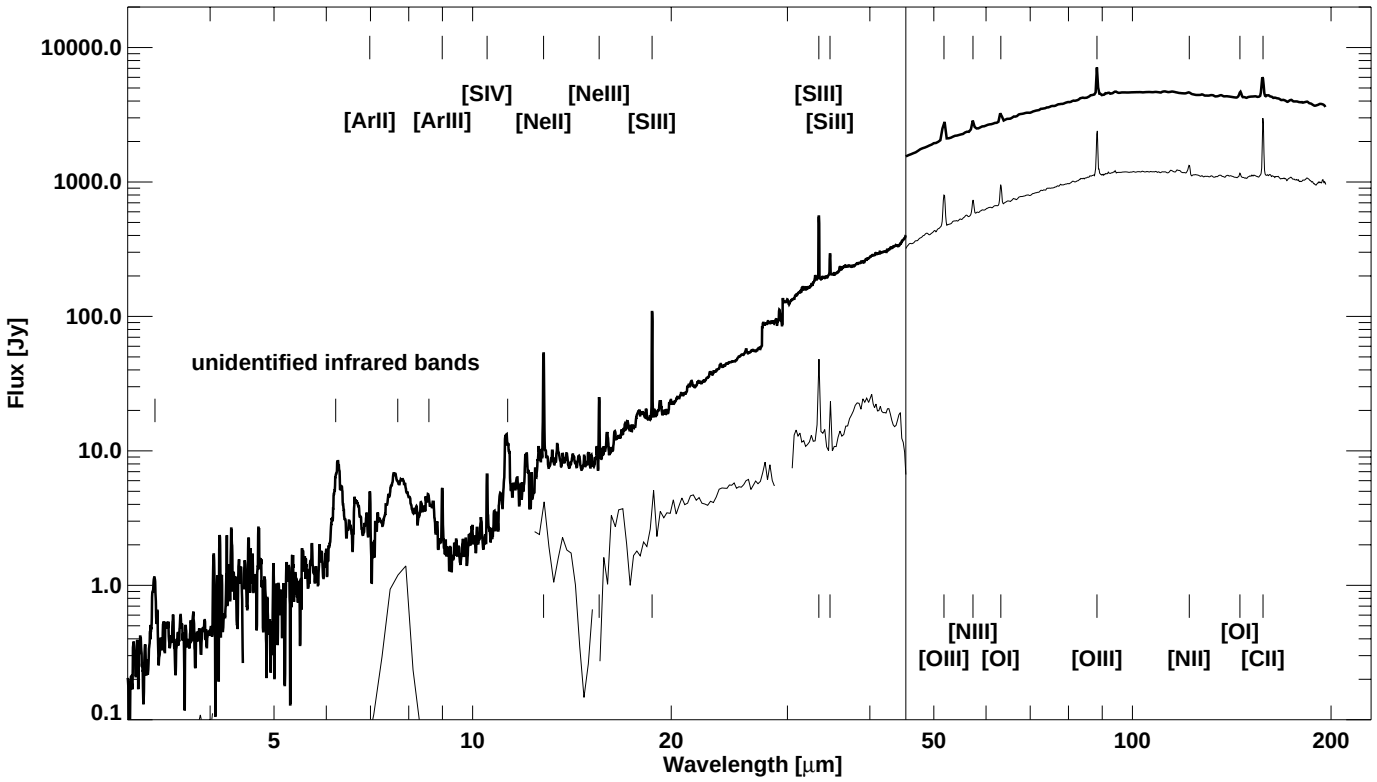

Fig. 2. In the left part of the figure the SWS spectrum is displayed, in the right part the LWS spectrum. The bold line displays the spectrum observed at the on-position, the thin line stands for the off-position. Where the thin line is missing the data reduction produced "negative" fluxes. The flux scale is the same in both parts of the figure.

IRAS-HiRes map at 100 μm plotted over an optical image of M 17 from the Digitized Sky Survey (DSS). The IRAS map demonstrates clearly the presence of emission from this condensation which can also be seen in the IRAS-HiRes maps at all other IRAS wavelengths. Compared to M 17-SW, M 17-North is much fainter at 12 and 25 μm than at 60 and 100 μm apparently indicating a considerably lower temperature. Gatley et al. (1979) determined a colour temperature of about 40 K in M 17-North while they observed temperatures between 50 and 120 K in M 17-SW. However, this colour temperature does not reflect the physical temperature of the dust particles because the non-thermal emission of very small grains (VSGs) also contributes to the emission up to 60 μm. The FIR luminosity of M 17-North, $6 \cdot 10^4\,\mathrm{L}_\odot$ (Gatley et al. 1979), could be provided by the stars in the centre of M 17, which also excite the H II region. M 17-North would not need any internal heating source, at least not of such brightness. This picture requires low extinction between M 17-North and the centre of M 17, which is in agreement with the observations (see also Gatley et al. 1979). On the other hand, the total radio flux measured by Wilson et al. (1979) would lead to a spectral type of a late O star if a single "internal" star would be the exciting source.

The detection of a compact dust core at millimetre wavelengths made the object an extremely interesting target for the study of star formation and the properties of the dust and molecule population in a cloud core. The data presented in this paper serve as the starting point for revealing the nature of M 17-North. The best set of information comes from a complete ISO spectrum covering the wavelength range between 2.4 and 200 μm using the ISO instruments SWS and LWS. These data are supplemented by ground-based observations. We present the first millimetre continuum map of the cloud core together with near-infrared and N-band imaging data in order to find the relation of cloud structure and stellar content.

The next section gives the details of the observations while in Sect. 3 the obtained data are presented. In Sect. 4 we discuss selected observational results as the unidentified infrared bands (UIBs), the fine structure lines, and the spectral energy distribution (SED). Finally the results are summarized in Sect. 5.

2. Observations

2.1. ISO observations

The observations were made with the short- and long-wavelength spectrometers (SWS/LWS) (de Graauw et al. 1996; Clegg et al. 1996) on board of the Infrared Space Observatory (ISO) (Kessler et al. 1996) within the guaranteed time programme YSO_MC. To obtain a spectrum over the full wavelength range of the two instruments, we chose the observing modes SWS01 and LWS01. These modes allow to take a full oversampled spectrum with a resolution of about $R = \lambda/\Delta\lambda \approx 200$ in 1848 s (1289 s) with SWS (LWS). In this mode the SWS reaches 1/8 of the instrument's nominal resolution which varies

with wavelength between R=1000 and R=2000. The LWS has a resolution between R=150 and R=300. The apertures of the two instruments are quite different. The SWS has three rectangular apertures with sizes ranging from $14''\times20''$ to $20''\times33''$. The width of the LWS beam is estimated to be $70''$ to $80''$ (FWHM). In order to have control over the background emission, an observation was performed at an off-position shown in Fig. 1. The coordinates (epoch: 2000) are for the on-position RA= $18^{\rm h}20^{\rm m}32\overset{\rm s}{.}7$, DEC= $-16^\circ01'42\overset{''}{.}6$ and for the off-position RA= $18^{\rm h}20^{\rm m}46\overset{\rm s}{.}9$, DEC= $-16^\circ03'45\overset{''}{.}5$.

The data reduction was partly done at the ISO Spectrometer Data Center (ISOSDC) at the MPE in Garching. The SWS data were reduced starting from the pipeline edited raw data (ERD) using the Interactive Analysis (IA) Software at the ISOSDC up to the Auto Analysis Result (AAR) (de Graauw et al. 1996). For the LWS products we started the data reduction with the pipeline AAR (Swinyard et al. 1996). Both AARs were further investigated with the ISAP software package distributed by the ISOSDC.

The preference of the interactive data reduction of the SWS spectra over the automatic pipeline reduction had several reasons. The automatic routines interpreted very intense, sharp lines as spikes caused by cosmic rays and removed them. In contrast, the interactive handling of the data avoids this and also improves the other steps in the data reduction, particularly the dark current subtraction and flat-fielding. Both instruments have problems with fringes when the source is extended, as it is the case with our molecular cloud core. We removed them using Fourier filtering as the frequency of the fringes were constant and easily detectable in wavenumber space.

2.2. Ground-based observations

Complementary to the ISO observations, the cloud core M 17-North was mapped in the 1.3 mm dust continuum emission. The observations were performed in February 1993 and in March 1997 at the IRAM 30m telescope on the Pico Veleta, Spain. In 1993 the telescope was equipped with the ^{3}He-cooled 7 channel bolometer array of the MPIfR Bonn and in 1997 with the 19 channel array. The equivalent bandwidth of the bolometer is about 50 GHz centred at a frequency of 236 GHz (λ_0=1.27 mm). The effective beamsize (HPBW) of the combined map is $12''$. The map covers a field of $3'\times4'$.

Near-infrared observations of the cloud core M 17-North were performed in March 1995 at La Silla, Chile. The IRAC2b camera was used together with the ESO/MPIA 2.2m telescope to image a field of $3'\times3'$ in the H- (1.65 μm) and K′-band (2.23 μm) with a pixel scale of 0.5″/pixel. The image is a mosaic of four images with offsets of $1'$. Each image is integrated 60 s and we reached a limiting magnitude (5σ) of roughly 18 mag in both bands. We determined the near-infrared (NIR) colour index $m_{\rm H-K'}$ of objects well detected in both bands. The result is shown in Fig. 5. In June 1997 the cloud core was searched for emission at 10 μm with the MIR camera MANIAC at the ESO/MPIA 2.2m telescope.

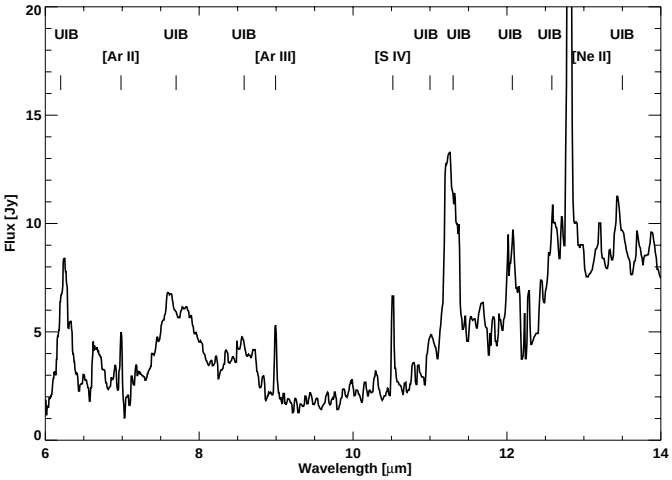

Fig. 3. The range of the UIBs in the SWS spectrum of M 17-North enlarged.

3. Results

3.1. ISO observations

Fig. 2 shows the complete SWS/LWS spectrum for the on- and off-position. The SWS "on-spectrum" and the LWS spectra are rebinned to a resolution of R=200. The SWS observation at the off-source position was performed with the same resolution as the measurement at the on-source position but with a shorter integration time resulting in a lower signal-to-noise ratio. A simple subtraction of the off-source measurement from the on-source data would introduce additional noise into the spectrum and is, therefore, not performed and both spectra are displayed separately (Fig. 2). The SWS "off-spectrum" is averaged over 0.2 μm wide bins.

The on-spectrum shows a number of relatively strong UIBs, fine-structure lines and Br α emission typical for ionized regions. In addition, we see a strong rise of the continuum at wavelengths longer than $\approx$15 μm. The data resemble the spectrum of the interface/molecular cloud region of M 17-SW (Cesarsky et al. 1996, Verstraete et al. 1996; see Sect. 4.1). The wavelength region of the spectrum with the distinct UIBs is shown enlarged in Fig. 3. The 6.2 μm UIB is relatively narrow. A weaker feature at 6.7 μm may not be real because of the stronger noise at this wavelength. We see a broad feature between 7.2 and 8.1 μm which has a double-hump structure present also in other ISO spectra (see, e.g., Roelfsema et al. 1996). The 8.6 μm band extends to 8.8 μm with a very low continuum up to the well-known 11.3 μm feature. This behaviour is similar to the behaviour seen in the ISO spectra of compact H II regions (Roelfsema et al. 1996). The depression in the 10 μm region could either be produced by silicate absorption or be just evidence for a very low continuum between molecular emission bands. In addition, we see two more known bands at 12.0 and 12.7 μm. The M 17-North spectrum shows a weak band at 13.5 μm that has been seen rarely in previous observations.

In case of the SWS observation, the background emission is only about 10% compared with the source emission. The lines in

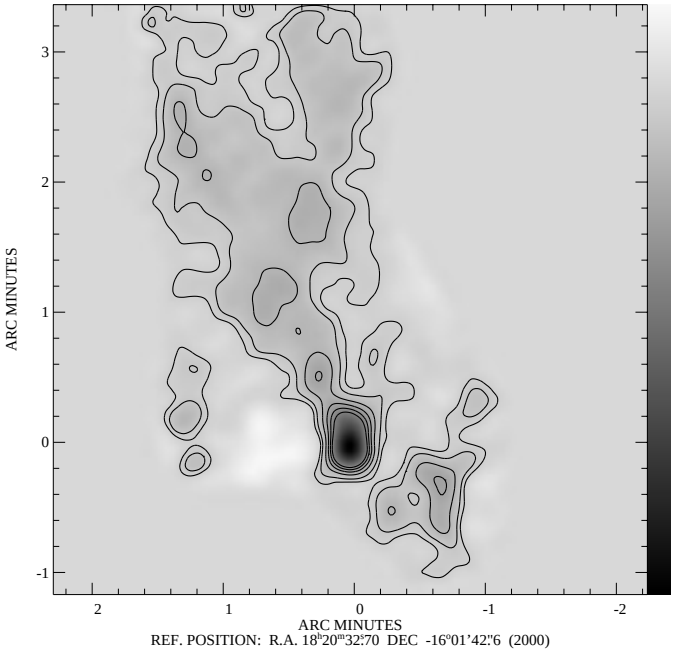

Fig. 4. M 17-North mapped with the bolometer arrays at the IRAM 30m telescope at 1.3 mm wavelength. The contour levels are 0.05, 0.1, 0.2, 0.3,... Jy/beam. The peak flux is 1.25 Jy/beam

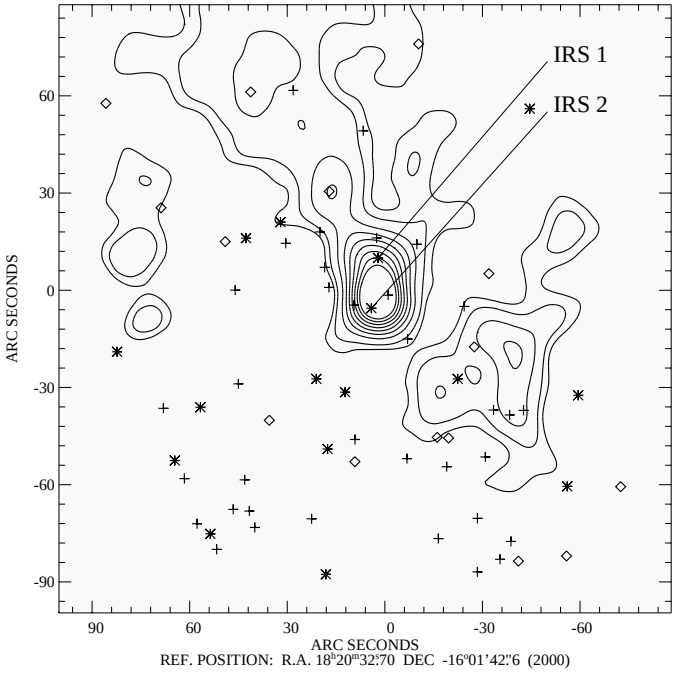

Fig. 5. The symbols mark the stars with flux measurements in the H- and K′-band. Here the colour index $m_{\mathrm{H-K'}}$ is shown. The asterisks denote the "reddest" stars with $m_{\mathrm{H-K'}}$ positive. The crosses stand for $m_{\mathrm{H-K'}}$ between -1 and 0 mag, and the diamonds for $m_{\mathrm{H-K'}}$ lower than -1 mag. The contours show the 1.3 mm continuum emission (cf. Fig. 4).

the off-source spectrum have about 20 to 30% of the flux of their counterparts in the on-source spectrum if they show up at all. In case of the LWS measurements, the off-source observation detected 25% of the source flux. The fine structure lines in the off-source measurement are all by factors from 2 to 4 less intense except for the 145.5 μm [O I] line with only 10% of the flux and the 121.9 μm [N II] line which has the same flux in both spectra within the uncertainties.

The SWS spectra display jumps around 30 μm due to the changing aperture of the SWS. The jump between the SWS and LWS spectrum is also due to the different aperture sizes as M 17-North is quite extended.

3.2. Millimetre continuum observations

The bolometer map of M 17-North (Fig. 4) shows a strong compact emission, $19'' \times 8''$ in size, elongated in N-S direction. The total flux coming from this compact core is 3.5 Jy. Assuming a gas-to-dust ratio of 150, a dust opacity of 1 cm^2/g at 1.3 mm, and a dust temperature of 40 K, the core has a mass of 200 $M_\odot$. A large region of emission extends from this compact source to the north with brightness varying between 0.1 and 0.2 Jy/beam emitting a total flux of 14.5 Jy. It covers a region of $220'' \times 80''$ in size. Assuming a temperature of 20 K and a dust opacity of 0.5 cm^2/g for the envelope, it has a mass of 4000 $M_\odot$. The dust opacities are taken from Ossenkopf & Henning (1994).

The main uncertainties for the mass estimate are the dust opacity and the dust temperature, which may both vary by a factor of 2. For lower temperatures, the derived masses are more sensitive to the assumed temperature values. Therefore, the envelope mass is uncertain by at least a factor of 4.

In addition to the main structure seen in the millimetre map, more cloud fragments can be seen. One fragment is located south-west of the core and emits 2.25 Jy. The other fragments can be found east of the main core and emit 0.93 Jy.

3.3. NIR and MIR observations

The NIR images shown in Fig. 5 reveal many sources in the region of M 17-North. However, only two red objects are located in the cloud core. The northern object has a H magnitude of 14.5 mag and a colour index of $m_{\mathrm{H-K'}}$=0.9 mag. We call this object M 17N-IRS1. The colour index of the southern source (M 17N-IRS2) is only $m_{\mathrm{H-K'}}$=0.1 mag, too low to be deeply embedded, though it is right at the millimetre peak. The fluxes measured in the H- and K′-band for IRS1 are 1.7 and 2.5 mJy, respectively. This source was also detected in the N-band. We measured a flux of 0.4 Jy in the N-band, while neither IRS2 nor any other 10 μm source were detected in the cloud core. IRS1 is not located at the mm peak flux position. However, its colour and the detection at 10 μm suggests that it is deeply embedded in the cloud core. We cannot exclude that there are even more deeply embedded sources not seen up to 10 μm.

4. Interpretation

4.1. Unidentified infrared bands

Seven years after the first observation of the UIBs in the spectra of astrophysical sources, Léger & Puget (1984) and Allamandola et al. (1985) suggested that these bands may be attributed to free polycyclic aromatic hydrocarbon (PAH) molecules heated by single photons. Another suggestion was that hydrogenated amorphous carbon (HAC) particles are the carriers of the UIBs. In this case, weakly linked aromatic islands in these solids are responsible for the UIB emission (Duley 1989). The aromatic islands have to undergo large temperature excursions. However, experimental and theoretical studies contradict the island model (Boutin et al. 1995). Recent experiments on nanoparticles produced IR spectra similar to the UIBs in position, width, and shape of the bands (Herlin et al. 1997; see also Schnaiter et al. 1997). This nanometre-sized carbon dust is a quite promising model for the carriers of the UIBs.

In recent studies of UIB spectra, small or larger PAH molecules (Mattila et al. 1996) over PAH clusters (Molster et al. 1996) up to coal grains (Guillois et al. 1996) are proposed as carriers of the features (and the continuum if present). In order to radiate in the wavelength region in question (3 to 16 μm) the particles must be heated transiently by single or multiple photon heating.

An exciting result of the ISO mission is the presence of UIBs in environments with weak UV radiation fields and the relative similarity of UIB spectra in these cases (see, e.g., Boulanger et al. 1996). Visual or even IR photons can excite the emission of the UIB carriers. To distinguish between PAH molecules or very small hydrocarbon particles one has to consider in detail the excitation and fluctuating temperatures based on the different heat capacities of the possible band carriers. Such a study has to be relied deeply on new laboratory experiments and is beyond the scope of this paper.

In case of strong radiation fields, the UIBs show a much wider variation in intensity ratios and shapes (Roelfsema et al. 1996; Beintema et al. 1996). The spectrum of M 17-North belongs more to this category. Furthermore, the strong rise of the continuum for wavelengths larger than 15 μm points to the emission from VSGs transiently heated by the radiation field (Désert et al. 1990).

Geballe (1997) divided the UIB spectra in four different classes. The spectrum of M 17-North falls into the most common class "A" because of its four principal UIBs at 3.3, 6.2, 7.7, and 11.3 μm.

In M 17-SW several positions from the H II-region to the molecular cloud have been observed with ISO-SWS (Verstraete et al. 1996). Comparing the SWS spectrum of M 17-North to the SWS spectra of M 17-SW our spectrum is similar to the spectrum of the interface region in M 17-SW concerning the relative band intensities and the high band-to-continuum ratio. Verstraete et al. (1996) stated that the intensity of most of the UIBs is not correlated to the 16 μm continuum which is characteristic for single photon heating. Towards the H II region the 8.7 μm band becomes more intense (higher than the 7.7 μm band) and correlates to the 16 μm continuum suggesting that the band originates from VSGs which dominate the continuum at these wavelengths. The band at 13.5 μm is also assigned to VSGs by Verstraete et al. (1996). A similar investigation of M 17-SW with ISOCAM led to the same results (Cesarsky et al. 1996). They suggested that these UIBs are carried by small aromatic grains or large PAHs being in an out-of-equilibrium thermal state. The strong continuum in the H II region is dominated by the emission of VSGs which are bigger than those particles responsible for the UIBs. From the inspection of our SWS spectrum (see Sect. 3.1), we conclude that in M 17-North the physical state of the UIB and continuum carriers should be similar to those in the interface region of M 17-SW observed by Verstraete et al. (1996) with SWS and at the position 3 observed by Cesarsky et al. (1996) with ISOCAM.

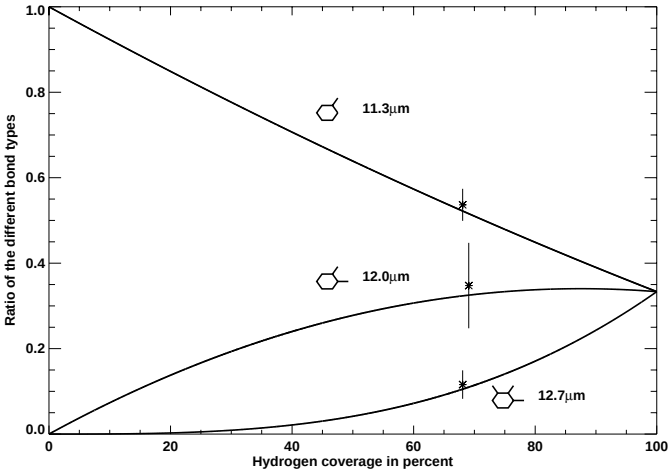

Fig. 6. The number of the three C–H bond types relative to the total number of C–H bonds as a function of fraction of the used bonding sites for hydrogen (Schutte et al. 1993). The stars indicate the ratio of bond types found from the band intensities in the spectrum of M 17-North. The star for the duo C–H mode is set a little apart to separate the error bars.

4.1.1. Hydrogen coverage of the polycyclic aromatic particles

The bands from 11 to 14 μm are formed by C–H out-of-plane vibrations in an aromatic system. The positions of those bands depend on the number of hydrogen atoms bound to one aromatic ring. There are single, two, three or four adjacent hydrogen atoms (solo, duo, trio, quarto bonds) resulting in features with ascending wavelengths. In the spectrum of M 17-North, these features may be ascribed to the bands located at 11.3, 12.0, 12.7, and 13.5 μm. Therefore, this spectral region provides a specific signature of the location of hydrogen on the aromatic carbon skeleton. For example, when coal matures from semi-anthracite to anthracite the duo, trio, and quarto bands almost vanish because of the release of hydrogen (Guillois et al. 1996). The same is expected if PAH molecules dehydrogenate and Schutte et al. (1993) have proposed a method to estimate the hydrogen coverage from the C–H out-of-plane bands. They derived the number of hydrogen in solo, duo, and trio bonds de-

pending on the hydrogen coverage neglecting the quarto bonds. The ratio of the different bond types in dependence of the total hydrogen coverage can be derived using statistical arguments only. Schutte et al. (1993) just assumed that every bond type is equally likely which is true for large PAHs ($n_{\rm C} \gtrsim 100$). If this assumption holds also for carbonaceous nanoparticles, this method should be equally applicable to VSGs. Assuming that the hydrogen atoms are randomly distributed over the available sites, the number of single, two, and three adjacent C–H bonds as a function of the hydrogen coverage are given by

$$n_{\rm H,1}(f_{\rm H})/n_{\rm H}(f_{\rm H}) = 1 - \frac{7}{9}f_{\rm H} + \frac{1}{9}f_{\rm H}^2, \quad (1)$$

$$n_{\rm H,2}(f_{\rm H})/n_{\rm H}(f_{\rm H}) = \frac{7}{9}f_{\rm H} - \frac{4}{9}f_{\rm H}^2, \quad (2)$$

$$n_{\rm H,3}(f_{\rm H})/n_{\rm H}(f_{\rm H}) = \frac{1}{3}f_{\rm H}^2, \quad (3)$$

where $n_{{\rm H},x}$ is the number of solo, duo, trio C–H bonds ($x = 1, 2, 3$) and $n_{\rm H}$ is the total number of C–H bonds. The quantity $f_{\rm H}$ is the fraction of the used bonding sites for hydrogen or in other words the relative hydrogen coverage.

The 11 to 14 μm band intensities in the M 17-North spectrum are derived by subtracting a straight baseline at the bottom of each band also if the band sits on a broad plateau. This avoids the difficulty of the uncertain heights of the plateaus. In the next step, the band intensities are divided by the intrinsic band strengths also given by Schutte et al. (1993) to obtain a value proportional to the number of bonds. To determine the ratios of the three bond types to the total number of C–H bonds, the value for each of the three bands is divided by the sum of the three. In Fig. 6 the asterisks display the relative number of bond types derived from the observations at the value for the hydrogen coverage where they fit best the functions. The result is a hydrogen coverage of about 70%.

4.2. Fine structure lines

Table 1 lists all detected fine structure lines (and Br α) with the measured wavelengths. The ground state of the respective atoms and ions displays fine structure splitting due to spin-orbit-coupling. All the fine structure lines result from forbidden transitions between the levels within the ground state.

Electron collisions excite the atoms/ions. We expect low excitation conditions because of the absence of lines from highly ionized species such as Ne V or O IV. Due to the small excitation energy, the fine structure lines are relative insensitive to the actual electron temperature. Only at low densities the temperature becomes more important. The species, where two lines could be observed, are good indicators for the electron temperature and density (Tab. 2) because the radiation is emitted by the same species and comes from the same area which means equal density of emitting atoms/ions and equal excitation conditions. The ratio of these line intensities is equal to the ratios of the respective emissivities. We use the calculations by Simpson (1975) for the emissivity coefficients j/N_eN_i of forbidden IR lines.

Table 1. Fine structure lines in the M 17-North spectrum. The given wavelengths are the observed ones.

λ [μm]	Name	λ [μm]	Name	λ [μm]	Name
SWS				LWS	
4.051	Br α	33.48	[S III]	51.78	[O III]
6.984	[Ar II]	34.81	[Si II]	57.30	[N III]
8.993	[Ar III]	36.00	[Ne III]	63.16	[O I]
10.52	[S IV]			88.40	[O III]
12.81	[Ne II]			122.0	[N II]
15.55	[Ne III]			145.5	[O I]
18.71	[S III]			157.8	[C II]

Table 2. Intensity ratios of the species with two transitions in the IR. The errors represent the uncertainty in the line fits and do not include systematic errors form the flux calibration.

Transition	Wavel. [μm]		Ratio (on)	Ratio (off)
[Ne III]	15.6	36.0	3.89 ± 0.8	–
[S III]	18.7	33.5	0.73 ± 0.03	0.53 ± 0.03
[O III]	51.8	88.4	0.96 ± 0.01	0.64 ± 0.01
[O I]	63.2	145.5	2.48 ± 0.12	9.02 ± 0.5

The intensity of the two [O III] lines are almost equal, which indicates an electron density of 100–200 cm^{-3} independent of the temperature. The intensity ratios of the [S III] transitions are more sensitive to the temperature. A temperature between 7000 K and 5000 K[1] and a density between 50 and 200 cm^{-3} reproduce the observed ratio. Sulphur is ionized more easily than oxygen (the ionization potential for the second ionization step of sulphur and oxygen are 23.33 eV and 35.12 eV, respectively), so that the radiation in the [S III] lines could originate from a less ionized region with a lower electron density. As an average, we estimate that the electron density amounts to 100 cm^{-3} and the electron temperature is about 5000 K around M 17-North.

The intensity ratios of the transitions of [Ne III] and [O I] given in Tab. 2 are at least by factors 3 and 4 smaller than predicted by the theory (Simpson 1975) for $\rm n_e > 10\,cm^{-3}$ and $T_e > 5000\,K$, respectively.

The same considerations for the lines in the off-source spectrum lead to a density of the order of 10 cm^{-3} at a low temperature. This value can be deduced from the [S III] and [O III] transitions. The ratio of the [O I] lines almost reaches 10 which is the correct value for low densities and temperatures. The [N II] line is not intrinsic to the spectrum of M 17-North as it is as bright in the off-source spectrum as in the on-source spectrum.

4.3. Radiative transfer for the continuum

We fitted the SED from the NIR up to the millimetre region by a spherically symmetric RT model. We used the RT code described in Manske et al. (1997). With this code it is now also possible to calculate the contribution from transiently heated VSGs as described by Manske & Henning (1997).

[1] 5000 K was the smallest temperature used by Simpson (1975).

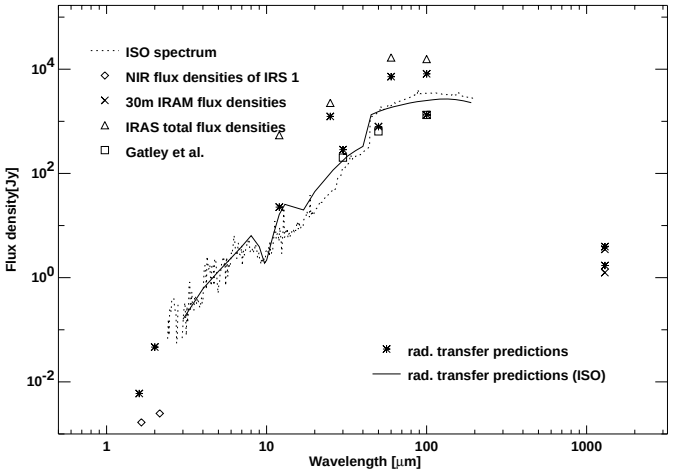

Fig. 7. Comparison of observations with predictions by the RT model.

Table 3. These parameters give a fairly good fit to the observations.

r_1	$2.4 \cdot 10^{17}$	cm	L	8000	$L_\odot$	A_V	80	mag
r_2	$4.8 \cdot 10^{18}$	cm	T	3000	K	M_{tot}	6000	$M_\odot$
n_H	$2.1 \cdot 10^5$	cm^{-3}	T_{out}	80	K	L_{tot}	$8 \cdot 10^4$	$L_\odot$

Gatley et al. (1979) pointed out that the FIR luminosity ($6 \cdot 10^4\,L_\odot$) of M 17-North can be explained by the radiation coming from the centre of M 17 taking into account the distance of 10′ and the extent of M 17-North of 4′. We should stress again that the total extent of M 17-North is larger than just the extent of the compact core seen in the millimetre emission. Therefore, our model includes an outer radiation field which provides almost all the luminosity of the cloud core and heats its outer regions. The outer radiation field is treated in an approximate way by a black body radiation field of the temperature T_{out}. We placed a heating source in the centre of the model cloud to explain the MIR flux. The central heating source is surrounded by a dust shell, which has a constant density n_H up to an radius r_1. From this radius on, the density decreases as r^{-1}. The dust shell ends at the radius r_2. With the parameters given in Tab. 3 the dust shell has a visual extinction of $A_V = 80$ mag and the gas mass of the model cloud including the extended envelope is 6000 $M_\odot$. The mass of the core is 100 $M_\odot$ (integrated up to an radius of 20″) in agreement with the rough estimates from the millimetre map. The parameters of the internal heating source are the temperature T and its luminosity L. The temperature T should only be taken as a characteristic temperature for the central heating region, it is not the effective temperature of an embedded star.

The dust model consists of amorphous carbon, graphite, and silicate particles following a size distribution $n(a) \propto a^{-4.1}$. The size of the transiently heated graphite and silicate particles ranges from 1 to 10 nm. The size of the amorphous carbon particles ranges from 0.015 to 0.120 μm and of the silicate particles from 0.030 to 0.240 μm. The optical properties for amorphous carbon are taken from Preibisch et al. (1993), for graphite from Draine (1985), and for silicate from Dorschner et al. (1995). A model with the parameters compiled in Tab. 3 gives a fairly good fit to the observations.

Fig. 7 shows the observed SED and the model SED. The total luminosity emitted by the model cloud is $8 \cdot 10^4 L_\odot$. In general, the observations do not reflect the total flux but refer to the beamsize. The asterisks denote the flux density which should be received in the different apertures of the observations.

In Fig. 7 the ISO spectrum (dotted line) is rebinned to a low resolution (R=100) and the off-source spectrum is subtracted. The solid line is the prediction of the model for the ISO observation. The overall structure of the spectrum is reproduced by the model but we were not able to produce such a big change of flux density due to the different apertures of SWS and LWS. Our model produces a flux a little too high between 15 and 45 μm and a little too low for wavelengths longer than 45 μm. The high optical depth of the model also results in the rapidly vanishing flux towards shorter wavelengths suggesting a much higher colour index for IRS1 than observed if it was in the centre of the core. The KAO measurements by Gatley et al. (1979) are well reproduced. The total fluxes coming from a region of $5' \times 5'$ size are estimated from IRAS HiRes maps. These fluxes are an order of magnitude higher than the ISO fluxes demonstrating the relatively large contribution from the molecular cloud envelope. Our model fails to explain the 12 μm emission from the envelope which is due to the simplicity of the assumed outer radiation field. The outer radiation field should be produced by the stars powering the H II region M 17. Their radiation will be processed by intervening material resulting in a broader SED than just a black-body curve. A "fine-tuning" of the shape of this radiation field makes no sense without additional observational constraints about its nature. Furthermore, the radiation hits M 17-North only from the south, whereas in the model an isotropic radiation field is assumed.

The observed fluxes at 1.3 mm are the peak flux density and the total flux density of 3.5 Jy emitted by the core (cf. 3.2). The asterisks again denote the predictions by the model which fit the observed data very well. In general, we can conclude that the RT code with VSGs reproduces the broad-band spectral energy distribution of M 17-North. The expected reddening from the model is higher than observed for IRS1, which points to a more complicated geometry which would especially influence the NIR part of the SED.

4.4. The central source

The core of M 17-North contains the embedded infrared source IRS1 which probably contributes to the total luminosity of M 17-North. Evidence for ionizing radiation and therefore for the presence of an early-type star comes from radio observations (Wilson et al. 1979), and our detection of the relevant fine structure lines and Br α emission.

However, the luminosity of the central core region ($19'' \times 8''$ in the millimetre map) is only 20% of the total luminosity. It was not possible to produce the relatively bright extended envelope

emission seen in the comparison of the IRAS/ISO data and the aperture effects in the ISO data without external heating in the RT model. Furthermore, the colour index $m_{\mathrm{H-K'}}$ of IRS1 had to be much higher than observed according to the RT calculations, if it would really be the central object of the cloud. The intensity of the Br α line and the fine structure lines may also be explained by the ionizing radiation field emitted from the central cluster in M 17. The intensity of this radiation field could reach 10^3 times the standard interstellar intensity around M 17-North taking into account the total luminosity of the OB cluster in M 17 and the geometric dilution.

5. Conclusion

We presented observational data from the NIR up to millimetre wavelengths of the cloud core M 17-North. The main issues discussed in the paper were the spectrum obtained by ISO including the UIBs and the fine structure lines and the analysis of the cloud core structure including the ground-based data and applying a radiative transfer code. This code also included the treatment of the emission from VSGs.

The detected features in the ISO spectrum can be summarized in the following way:

1. UIBs: The UIBs are carried by small aromatic hydrocarbon grains or large molecules transiently heated. They have a hydrogen coverage of 70% in M 17-North.
2. Fine structure lines: Using the line ratios we estimated an electron density and temperature of 100 cm^{-3} and 5000 K, respectively. The electron temperature is relatively uncertain due to the insensibility of these fine structure lines to this parameter.
3. Continuum: It starts to dominate the spectrum at wavelengths longer than 15 μm and still originates from transiently heated grains. The continuum reaches its maximum at about 100 μm.

We detected an infrared source at NIR wavelengths, which is also "visible" at 10 μm. Though IRS1 might not be in the centre of the core of M 17-North, its detection at 10 μm and its colour index typical for an embedded object is the first direct sign of a young stellar object in M 17-North and already on-going star formation. With the RT model we tried to reproduce the continuum radiation observed by ISO and the other telescopes. The model shows that most of the extended FIR luminosity observed is provided by outside heating, namely by the exciting stars in the centre of M 17. The outer radiation field cannot explain the NIR/MIR flux seen by ISO. We had to include a central source with a luminosity of 8000 $\mathrm{L}_{\odot}$. As this is only 10% of the total luminosity, this value is relatively uncertain.

Planned ISOCAM observations similar to the observations of M 17-SW (Cesarsky et al. 1996) will help to refine the analysis of M 17-North as we will be able to determine if the core is irradiated from the south or is powered from inside. The spatial variation of the UIBs, of the fine structure lines, and of the continuum will point to the energy source.

Acknowledgements. Two of the authors (R. K. and R. L.) acknowledge support through the BMBF-Verbundforschung Astronomie / Astrophysik grant No. 50 OR 9414 9. We thank Th. Lehmann for performing the 10 μm observations, R. Zylka for providing the 1993 bolometer map of M 17-North and V. Manske for helping with the RT modelling. We acknowledge support from the ISO Spectrometer Data Centre at MPE Garching, funded by DARA under grant 50 QI 9402 3.

References

Allamandola L. J., Tielens A. G. G. M., Barker J. R., 1985, ApJ 290, L25
Beintema D. A., van den Ancker M. E., Molster F. J., et al., 1996, A&A 315, L369, ISO special issue
Boulanger F., Reach W. T., Abergel A., et al., 1996, A&A 315, L325, ISO special issue
Boutin A., Léger A., Désert F. X., Boissel P., d'Hendecourt L., 1995, MNRAS 274, 435
Cesarsky D., Lequeux J., Abergel A., Perault M., Palazzi E., Madden S., Tran D., 1996, A&A 315, L309, ISO special issue
Chini R., Elsässer H., Neckel Th., 1980, A&A 91, 186
Clegg P. E., Ade P. A. R., Armand C., et al., 1996, A&A 315, L38, ISO special issue
de Graauw Th., Haser L. N., Beintema D. A., et al., 1996, A&A 315, L49, ISO special issue
Désert F. X., Boulanger F., Puget J. L., 1990, A&A 237, 215
Dorschner J., Begemann B., Henning Th., Jäger C., Mutschke H., 1995, A&A 300, 503
Draine B. T., 1985, ApJS 57, 587
Duley W. W., 1989, The IR emission features and hydrogenated amorphous carbon (HAC) particles. In: L. J. Allamandola and A. G. G. M. Tielens (eds.), Interstellar Dust, Proc. IAU Symp. 135, Kluwer Acad. Publ., Dordrecht, pp 141–146
Gatley I., Becklin E. E., Sellgren K., Werner M. W., 1979, ApJ 233, 575
Geballe T. R., 1997, Spectroscopy of the unidentified infrared emission bands. In: Y. J. Pendleton and A. G. G. M. Tielens (eds.), From Stardust to Planetesimals, Vol. 122 of *ASP Conference Series*, pp 119–128
Guillois O., Nenner I., Papoular R., Reynaud C., 1996, ApJ 464, 810
Herlin N., Bohn I., Reynaud C., Cauchetier M., Galvez A., Rouzaud J.-N., 1997, A&A, in press
Kessler M. F., Steinz J. A., Anderegg M. E., et al., 1996, A&A 315, L27, ISO special issue
Léger A., Puget J. L., 1984, A&A 137, L5
Manske V., Henning Th., 1997, A&A, submitted
Manske V., Henning Th., Men'shchikov A., 1997, A&A, in press
Mattila K., Lemke D., Haikala L. K., et al., 1996, A&A 315, L353, ISO special issue
Molster F. J., van den Ancker M. E., Tielens A. G. G. M., et al., 1996, A&A 315, L373, ISO special issue
Ossenkopf V., Henning Th., 1994, A&A 291, 943
Preibisch Th., Ossenkopf V., Yorke H. W., Henning Th., 1993, A&A 279, 577
Roelfsema P. R., Cox P., Tielens A. G. G. M., et al., 1996, A&A 315, L289, ISO special issue
Schnaiter M., Mutschke H., Dorschner J., Henning Th., Salama F., 1997, ApJ, in press
Schutte W. A., Tielens A. G. G. M., Allamandola L. J., 1993, ApJ 415, 397
Simpson J. R., 1975, A&A 39, 43

Stutzki J., Stacey G. J., Genzel R., Harris A. I., Jaffe D. T., Lugten J. B., 1988, ApJ 332, 379
Swinyard B. M., Clegg P. E., Ade P. A. R., et al., 1996, A&A 315, L43, ISO special issue
Verstraete L., Puget J. L., Falgarone E., Drapatz S., Wright C. M., Timmermann R., 1996, A&A 315, L337, ISO special issue
Wilson T. L., Fazio G. G., Jaffe D., Kleinmann D., Wright E. L., Low F. J., 1979, A&A 76, 86